RSC Sustainability

ROYAL SOCIETY OF CHEMISTRY

PAPER

View Article Online
View Journal | View Issue

Cite this: *RSC Sustainability*, 2024, **2**, 2377

Environment-friendly acids for leaching transition metals from spent-NMC532 cathode and sustainable conversion to potential anodes†

Anjali V. Nair, Silpasree S. Jayasree,‡ Dona Susan Baji, Shantikumar Nair and Dhamodaran Santhanagopalan *

For a clean and sustainable world, energy storage systems like Li-ion batteries (LIBs) will play a vital role due to their wide range of applications. The exponential growth of batteries will lead to the generation of a substantial number of failed batteries in the near future. As a consequence, recycling will play a crucial role to reduce e-waste and to scale down the mining of virgin materials. Herein, we demonstrate a strategic approach to reduce e-waste and effectively reuse the same materials by regenerating batteries, enabling a circular economy. The study focuses on the recycling and regeneration of $LiNi_{0.5}Mn_{0.3}Co_{0.2}O_2$ (NMC532) cathode material *via* a hydrometallurgical process with two different environmentally friendly acids. The regenerated materials were characterized by X-ray diffraction, transmission electron microscopy and X-ray photoelectron spectroscopy. Regenerated mixed metal phosphide and oxide anodes exhibited excellent electrochemical performance in an LIB system. This work opens up the scope for a simple and scalable approach to develop the recycling and regeneration of NMC batteries, which will facilitate a circular economy, thereby leading the way for more developments in this field.

Received 30th April 2024
Accepted 24th June 2024

DOI: 10.1039/d4su00209a

rsc.li/rscsus

Sustainability spotlight

Increasing demand for energy storage technologies to be used in electronic gadgets to electric vehicles (EVs) to grid storage has led to advanced Li-ion battery technologies. With the increasing use of Li-ion batteries, resource exploration and extraction of lithium and transition metals have reached new heights. While the deployment of EVs has the aims of minimizing CO_2 emissions and addressing climate change issues (SDG 7 & 13), the processing of batteries is still a concern. This has necessitated the development of sustainable processes for material development and battery fabrication. Another aim is to recycle end-of-life batteries (SDG 12) which are urban mines for lithium and transition metals. In this context, we have developed sustainable alternatives in the form of environmentally friendly acids for mixed transition metal leaching from spent Li-ion batteries (SDG 12). As a proof-of-concept, a $LiNi_{0.5}Mn_{0.3}Co_{0.2}O_2$ (NMC532) cathode from a failed commercial Li-ion battery has been recycled in the form of metal oxalates. Subsequently, the metal oxalates have been converted to metal phosphides and metal oxides as fresh Li-ion battery anodes. Also, high energy density full-cells with the best performing anodes *vs.* high voltage $LiNi_{0.5}Mn_{1.5}O_4$ cathode have also been demonstrated (SDG 7).

1. Introduction

In the last three decades, the growth of lithium-ion batteries (LIBs) has been prolific, commencing with small pocket devices and leading to large automobile applications due to their high energy density, zero memory effect, and high energy efficiency.[1–3] The demand for LIBs is increasing globally and is expected to grow from 500 GW h per year in 2019 to more than 2500 GW h per year in 2030. In accordance with the statistical data , the production of electric vehicles will possibly rise from 10 million in 2020 to more than 30 million in 2030, considering that 41% of vehicles registered in 2020 were EVs. However, the increase in manufacturing and utilization will correspondingly pave the way for the substantial generation of electronic waste.[4–6] As the world is becoming electrified, environmental concerns regarding battery disposal and e-waste management are gaining importance. Technological solution towards sustainability including, reuse and recycle to reduce wastage of resources is growing.[7] According to Zhao *et al.*,[8] in China alone, battery scrap is expected to reach 0.78 million tons **in** 2025. To avoid metal contamination to water bodies and soil, to improve human health and to reduce carbon footprints, the recycling and recirculation of retired batteries are important. Furthermore, by 2035, all industries have to ensure that at least 20% of the cobalt, 10% of the lithium, and 12% of the nickel in

Amrita School of Nanosciences and Molecular Medicine, Amrita Vishwa Vidyapeetham, Kochi 682041, India. E-mail: dsgopalan20710@aims.amrita.edu

† Electronic supplementary information (ESI) available. See DOI: https://doi.org/10.1039/d4su00209a

‡ Present Address: VITO (Flemish Institute for Technological Research), Sustainable Materials, Boeretang 200, 2400 Mol, Belgium.

batteries come from reused materials.[9] Additionally, this will bring down the utilization of virgin metals and allow the reintroduction of processed materials, which will promote environmental conservation and protection. The main challenge for recycling is the second and subsequent level commercial application of spent LIBs. Consequently, flexible and adaptive recovery technologies will make battery recycling both ecologically and environmentally sustainable.[10–12]

Lithium nickel manganese cobalt oxide, $LiNi_{0.5}Mn_{0.3}Co_{0.2}O_2$ (NMC532), has emerged as a high-capacity and low-cost cathode compared to Co-rich, lithium cobalt oxide ($LiCoO_2$). NMCs are mainly deployed in electric vehicles, power tools, portable gadgets, grid energy storage *etc.* Furthermore, a higher nickel content helps to reduce the size of a battery by maintaining capacity without compromising voltage.[13–15] The recycling of an NMC cathode is promising to mitigate the availability of limited resources, to avoid the toxicity of metals when dumped into the environment and moreover to monetize society.[16–18] Even though this multi-element material exhibits the best performance, recycling and recovery are slightly risky because it exists as a mixed metal form. Depending on the complexity and composition of the materials, recycling can be carried out both physically and chemically. The main steps of the recycling process are a physical or pretreatment process, a chemical or extraction process and a product preparation process.[19–21] The initial step, the pretreatment process, includes dismantling of the battery, and separation of the cathode, anode, separator *etc.*, which are done manually and mechanically inside an inert atmosphere. Methods like solvent dissolution, ultrasonic assistance, thermal treatment, mechano-chemical methods *etc.* are employed to separate the anode from copper foil and the cathode from aluminum foil, which are adhered by polyvinylidene fluoride (PVDF) or polytetrafluoroethylene (PTFE) binders.[22] The most crucial part of the whole battery recycling processes is the transformation of the solid material to its liquid (dispersion) or any other form (alloy), which happens at the extraction stage. The extraction methods are mostly chemical processes like hydrometallurgy, pyrometallurgy, bio-metallurgy and direct recycling.[23,24] Due to its lower energy consumption at lower temperatures and good efficiency, hydrometallurgy is the best-known process which has been used for the longest time in the field of metal recovery from spent LIBs. The main processes coming under hydrometallurgy are leaching, solvent extraction and precipitation.[25,26] Pyrometallurgy or smelting is the reduction of valuable metals using high temperature. Although it is a simple technique, the process releases toxic gases and lithium cannot be extracted. The most relevant and promising technique is bio-metallurgy; because it works under mild reaction conditions, leaching can be promoted by microbial activity and is a cost-effective[27,28] but slow process. Direct recycling, the most industry-based technique, is a non-destructive and emerging technique in the field of recycling EV batteries. It includes mechanical, electrochemical, cathode-to-cathode and cathode healing techniques without the decomposition of the cathode material.[29] As discussed above, hydrometallurgy is the most widely used technique and it involves leaching with organic and inorganic acids along with H_2O_2 as reducing agent. Table 1 gives a list of leaching processes with different acids and their respective products from the literature.

Most of the literature concentrates on recycling the cathode into a fresh cathode; the transformation of metal phosphides (or oxides) as the anode has mostly been neglected. So, the main focus of this work is to recycle the valuable metals from a spent-NMC cathode and regeneration to mixed metal oxides/phosphides for use as an Li-ion battery anode but excluded Li-extraction. Table 1 shows a list of the literature that uses sulfuric acid or hydrochloric acid for leaching metals from spent batteries. It is well known that these two are strong acids and are not environmentally friendly. Finding alternative environmentally friendly acids without compromising leaching efficiency is the need of the hour. Most of the literature concentrates on HCl, H_2SO_4, HNO_3 *etc.* for leaching transition metals and achieving good efficiency. But these acids after leaching produce toxic gases like nitrogen and sulfur oxides, chlorine *etc.* and acidic waste water, which actually pollutes the soil and aquatic systems. So, in order to protect and sustain the ecological balance, this work uses organic acids, ionic liquids *etc.* In the case of *p*-toluenesulfonic acid (*p*-TSA) and sulfamic acid (SA) very much less research has been done in the recycling field, especially for the leaching of transition metals.[43,44] *p*-TSA is a strong organic acid and it is used as a hydrogen bond donor of deep eutectic solvents, which are reported to be economically and environmentally sustainable agents. It has a higher degree of selective recovery of metals, its water solubility limit is good and it is cost effective. The leaching efficiency is also comparable with that of other leachants. This acid is not harmful either to living systems or to non-living systems and the production of harmful gases is relatively minimal.[43–46] Mostly in the case of organic acids, the functional groups play a major role. Since *p*-TSA has sulfonyl groups, it ionizes completely in an aqueous medium and produces H^+ ions faster than other acids. Similarly, the ionic liquid SA is also employed because of its strong leaching capability with metals. SA is a neutral acid with a low corrosion rate, but it exhibits a strong acidic nature in an aqueous medium without producing toxicity or harmful effects to either the environment or human beings. During the process it exhibits stable characteristics with very much less energy consumption. So, comparing these two acids with HCl and H_2SO_4 environmentally, economically and experimentally, these acids are feasible, non-toxic, show low corrosiveness and are efficient at leaching metals.[43–48] Herein, we have demonstrated a simple, facile approach for recycling an NMC532 cathode with the aid of two different acids, namely *p*-TSA and SA, respectively. These acids can be used for leaching transition metals from an NMC532 cathode and subsequently form mixed metal oxalates. Oxalates can be further processed to form mixed metal phosphides and/or metal oxides. This technique is a simple and scalable approach to recycling NMC compounds, which will pave the way for more advances in this area of research. To the best of our knowledge, this is the first report on the usage of *p*-TSA and SA for mixed metal leaching from a spent NMC cathode.

Table 1 Comparison of metal leaching acids reported in the literature

Sl no.	Leachants	Processes	Products obtained	Reference
1	$HCl + H_2SO_4 + H_2O_2$	Leaching Precipitation	Li_2CO_3 Co-precipitates of Co–Ni–Mn hydroxides	16
2	$LFP + H_2SO_4 + FePO_4.2H_2O$	Leaching Induced crystallization	Li_2CO_3 Co-precipitates of Co–Ni–Mn	18
3	$H_2SO_4 + H_2O_2$	Leaching Solvent extraction Electro winning	Cobalt carbonate-$CoCO_3$	30
4	$H_2SO_4 + H_2O_2$	Sulfation roasting Leaching	Li_2SO_4	31
5	Oxalic acid	Leaching Selective precipitation	Co–Ni oxalate	32
6	$H_2SO_4 + H_2O_2$	Ultra sonication Leaching Micro emulsion	MnO_2 $CoCO_3$	33
7	Acetic acid + H_2O_2	Leaching Precipitation	Co-precipitation of Co–Ni–Mn hydroxide Li_2CO_3	34
8	$H_2SO_4 + H_2O_2$	Leaching Solvent extraction Precipitation	$Co(OH_2)$ $Mn(OH_2)$ $Ni(OH_2)$ Li_2CO_3	35
9	Formic acid + H_2O_2	Leaching Precipitation	Li_2CO_3 Co- precipitation of Co–Ni–Mn hydroxides	36
10	Lemon juice	Leaching Selective precipitation (pH dependent)	CoC_2O_4 $MnCO_3$ $NiCO_3$ Li_2CO_3	37
11	$H_2O + H_2SO_4$	Reduction roasting Carbonated water and acid leaching Evaporation Solvent extraction	Li_2CO_3 $NiSO_4 \cdot 6H_2O$ $CoSO_4 \cdot 7H_2O$ $MnSO_4 \cdot H_2O$	38
12	$H_2SO_4 + H_2O_2$	Leaching Hydrometallurgy Precipitation	$CoC_2O_4H_2O$ Li_2CO_3	39
13	$H_2SO_4 + NaHSO_3$	Leaching Hydrometallurgy Precipitation	CoC_2O_4 $MnCO_3$ $NiCO_3$ Li_2CO_3	40
14	Citric acid + H_2O_2	Leaching Hydrometallurgy Selective precipitation	CoC_2O_4 $MnSO_4$ $NiCl_2$ Li_3PO_4	41
15	$HCl + H_2O_2$	Leaching Recovery	Ni–Co–Mn carbonate	42

2. Experimental section

2.1. State of recovered material

2.1.1. Pretreatment process. A failed NMC532 (S-NMC) laptop battery was placed in an argon-filled glove box (Mbraun), where it was disassembled in order to prevent it catching fire. The graphite anode and NMC cathode were separated along with the respective metal foils. In order to remove the cathode binder, the cathode material was gently scraped off the aluminum foil and washed once with 1-methyl-2-pyrrolidone (NMP, Sigma-Aldrich) and then twice with distilled water using a centrifuge (HERMILE Z326). It was then kept in an 80 °C oven overnight and the dried material was named spent NMC (S-NMC), for use in further experiments.

2.1.2. Leaching process. Leaching is the extraction of metals in soluble form, by using a suitable leachant and reducing agent. Here the leaching is done with two inorganic acids, namely, *p*-toluenesulfonic acid, $C_7H_8SO_3 \cdot H_2O$ (*p*-TSA, SRL, 99% pure) and sulfamic acid, H_3NSO_3 (SA, SRL, 99% pure). The optimized conditions for leaching using both the acids are 0.9 vol% H_2O_2 (MERCK, 30%) concentration, 1 M acid concentration, solid-to-liquid ratio of 20 g L^{-1}, at 70 °C for 60 minutes with continuous stirring. The leaching is conducted in a necked round-bottom flask fitted with a condenser to avoid evaporation of the acids.[49] After 60 minutes, black colored solutions with some residues were formed with a pH of 1, that is highly acidic.

2.1.3. Precipitation of oxalates. This leachate solution was taken for precipitation, using ammonium oxalate

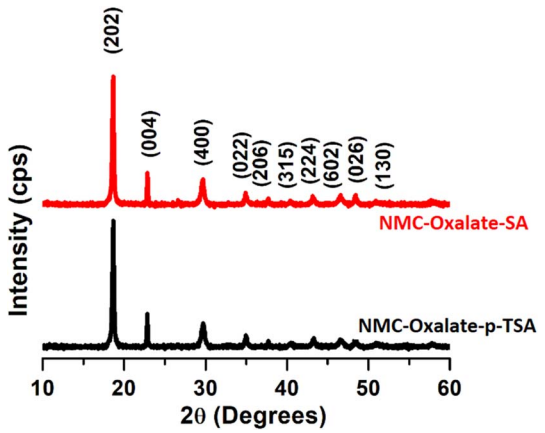

Fig. 1 XRD spectra of *p*-TSA and SA leached mixed metal oxalates.

($(COONH_4)_2 \cdot H_2O$, Nice Chemicals, India). The leachate solution was transferred to a clean beaker and kept under stirring. After a few minutes, the required amount of ammonium oxalate was added and kept under stirring for 30 minutes at an agitation speed of 300 rpm at room temperature. A white-grey colored precipitate was formed, which was filtered using a vacuum filtration pump (Genetix) and washed with water two or three times, to wash lithium out. The residue was then kept in an 80 °C oven for around 12 hours to dry. The obtained powder was cobalt–nickel–manganese oxalate ($Ni_5Mn_3Co_2(C_2O_4)$), which was weighed out and used for further processing.[32,50] For each acid the same precipitation process was repeated and labeled as mixed metal oxalates for further procedures.

2.1.4. Conversion of S-NMC oxalates to mixed metal phosphides. The recycled mixed metal oxalates were further regenerated to mixed metal phosphides by a vapor-phase conversion reaction using sodium hypophosphite. Both precursors were precisely weighed out in a ratio of 1 : 4 before being transferred to two clean, dry crucibles. They were then put inside a quartz thermal tube furnace (Delta Power Controls, India) for thermal annealing, where the thermal tubes were kept 5 cm apart inside. A regeneration gas, a mixture of argon and hydrogen gases, was provided for the process at a flow rate of 10% for about two hours at a temperature of 400 °C. Before the reaction the color of mixed metal oxalate was grey and for sodium hypophosphite it was white, but after annealing, the colors of the formed mixed metal phosphide and sodium hypophosphite were black and orange, respectively. Phosphidation can be confirmed by the color change and then it is weighed to prepare it for cell fabrication. Hence the obtained samples were named *p*-TSA-MP and SA-MP, respectively, derived from *p*-TSA and SA mixed metal oxalates.

2.1.5. Conversion of S-NMC oxalate to mixed metal oxides. The second step involved keeping a certain quantity of mixed metal oxalate samples for calcination at 500 °C for two hours at a rate of 5 °C min^{-1}. According to the leaching acids utilized, the mixed metal oxalates that were produced were given the names *p*-TSA-MO and SA-MO.

2.2. Structural and electrochemical characterization

The crystal structure of the recycled and regenerated materials was identified using X-ray diffraction analysis (XRD: D2 Phaser, 2nd generation, Bruker, Germany), where the Cu $K_{\alpha 2}$ signals and background subtraction were carried out using the EVA default program for XRD data mentioned in this work. Some of the oxalates and phosphides were characterized using a Bruker AXS D8 Advance (Germany) carried out at STIC, CUSAT. The weight ratio and thermal stability of the oxalate samples were studied using thermal gravimetric analysis (TGA, STA7200, Hitachi, Japan). Morphological characterization was supported by field emission scanning electron microscopy (FESEM, JSM-6490LA, Jeol, Japan) and transmission electrode microscopy (TEM, Tecnai G^2, FEI, Netherland) for all samples except *p*-TSA-MP where it was done at IIT Madras, (Jeol, F200, Japan). Elemental identification using energy dispersive X-ray analysis (JSM-6490LA, Jeol, Japan) and X-ray photoelectron spectroscopy (XPS, Kratos, Axis Ultra, UK) was utilized for surface chemical analysis, in which the X-ray source was Al Kα.

To test the performance and capacity of the prepared recycled mixed metal phosphides, the primary step is slurry casting. In a clean, dried-out mortar and pestle, equal parts of the active ingredients, carbon black 65 (Timical super 65), and polyacrylic acid were added in a ratio of 70 : 20 : 10. It was thoroughly

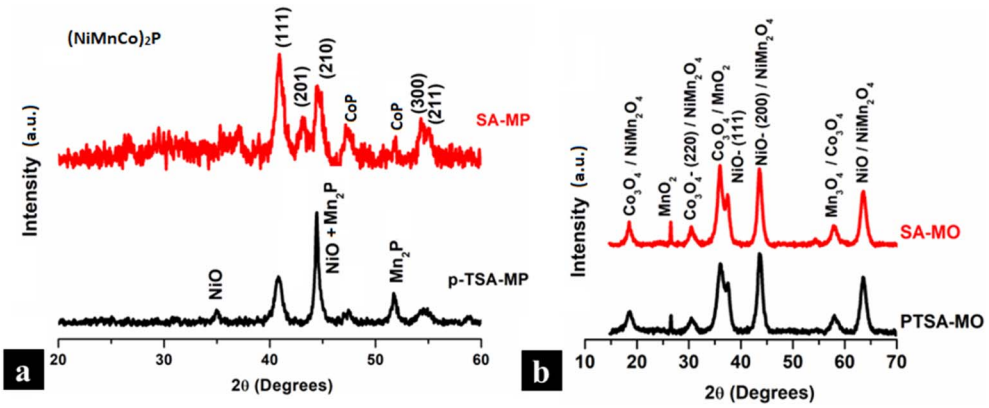

Fig. 2 XRD spectra of (a) mixed metal phosphides and (b) mixed metal oxides derived from *p*-TSA and SA leached mixed metal oxalate samples.

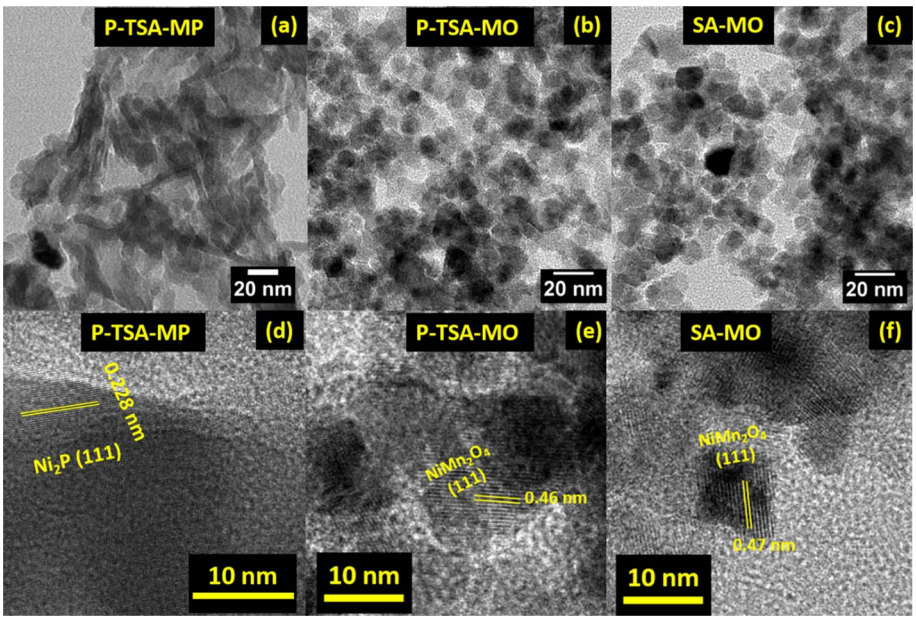

Fig. 3 (a–c) Low-magnification and (d–f) high-resolution TEM images of *p*-TSA-MP, *p*-TSA-MO and SA-MO, respectively.

blended and combined, and then using 100% ethanol as a solvent, it was turned into a slurry. Slurry casting of mixed metal oxide anodes was undertaken with respective amounts of the active materials, multiwalled carbon nanotubes (CNT) and lithium polyacrylate (LiPAA) as binder and conductive polymer, in a ratio of 75 : 15 : 10, along with deionized water as solvent. All the samples were kept for drying in an IR lamp oven (Panasonic Taiwan Co., Ltd), which maintained a temperature of 80 °C, for 15 minutes. Electrode loadings were typically 0.9 ± 0.2 mg cm^{-2} and used for assembling Swagelok cells inside an Ar-filled glove box, in which the O_2 and H_2O were maintained below 1.0 ppm using 1 M $LiPF_6$ in EC : DMC (1 : 1) as electrolyte, and the cells were made for each acid-prepared sample. Material testing and electrochemical analysis were carried out using a BioLogic system (BioLogic Science Instruments, USA) by fabricating half-cells and full-cells tested within potential windows of 0.01–3.0 V and 1.0–5.0 V, respectively.

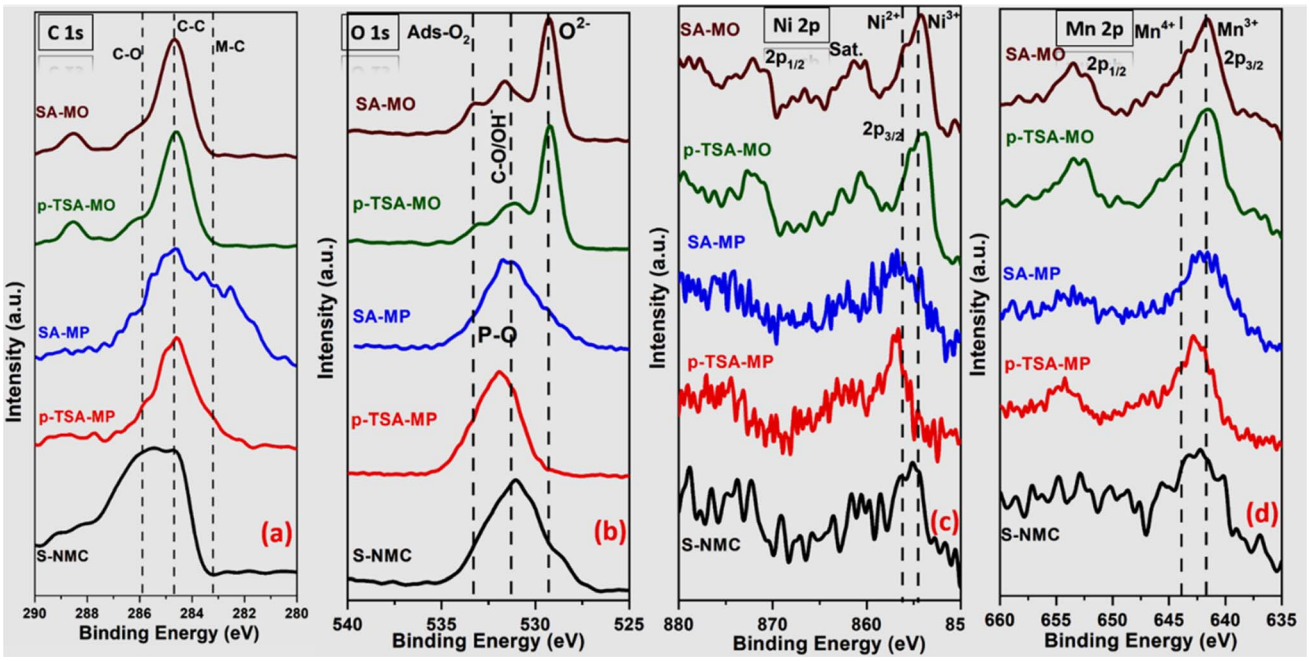

Fig. 4 XPS images of (a) C 1s, (b) O 1s, (c) Ni 2p and (d) Mn 2p of S-NMC and all four mixed metal phosphides and oxides regenerated from mixed metal oxalates.

3. Results and discussion

3.1. Transition metal oxalates leached from a spent-NMC532 cathode

The S-NMC532 XRD data (Fig. S1†) indicates that the O3-type layered oxide was consistent with the $R\bar{3}m$ space group. While the layered crystalline structure of S-NMC is maintained as indicated by the peak split of (006)/(102) at a 2θ value of 38° and (108)/(110) at 65°,[51] a high degree of cation mixing can be observed from the (003)/(104) peak intensity ratio (which is close to 1 in the S-NMC532). Fig. 1 shows that the XRDs of NMC-oxalates leached using *p*-TSA and SA are consistent with the XRD of mixed metal oxalates.[46] The highest peak is at a 2θ value of 19°, corresponding to (202). The XRD clearly proves that the single phase of NMC oxalates exists as the Ni-rich $(Ni_{0.5}Mn_{0.3}Co_{0.2})C_2O_4$ form.[52]

3.2. State of recycled anode materials

Fig. 2(a) shows the XRD of mixed metal phosphides leached out from *p*-TSA and SA, respectively, studied in the 2θ range of 20–60°. The XRD patterns of metal phosphides have an intrinsically poor signal-to-noise ratio along with surface oxidation or phosphate formation, as reported in the literature.[53–55] It may be observed from the XRD that a mixed metal phase of $(Ni_{0.5}Mn_{0.3}Co_{0.2})_2P$ phosphide structure exists after phosphidation of the oxalate, with some quantity of secondary oxide phases (such

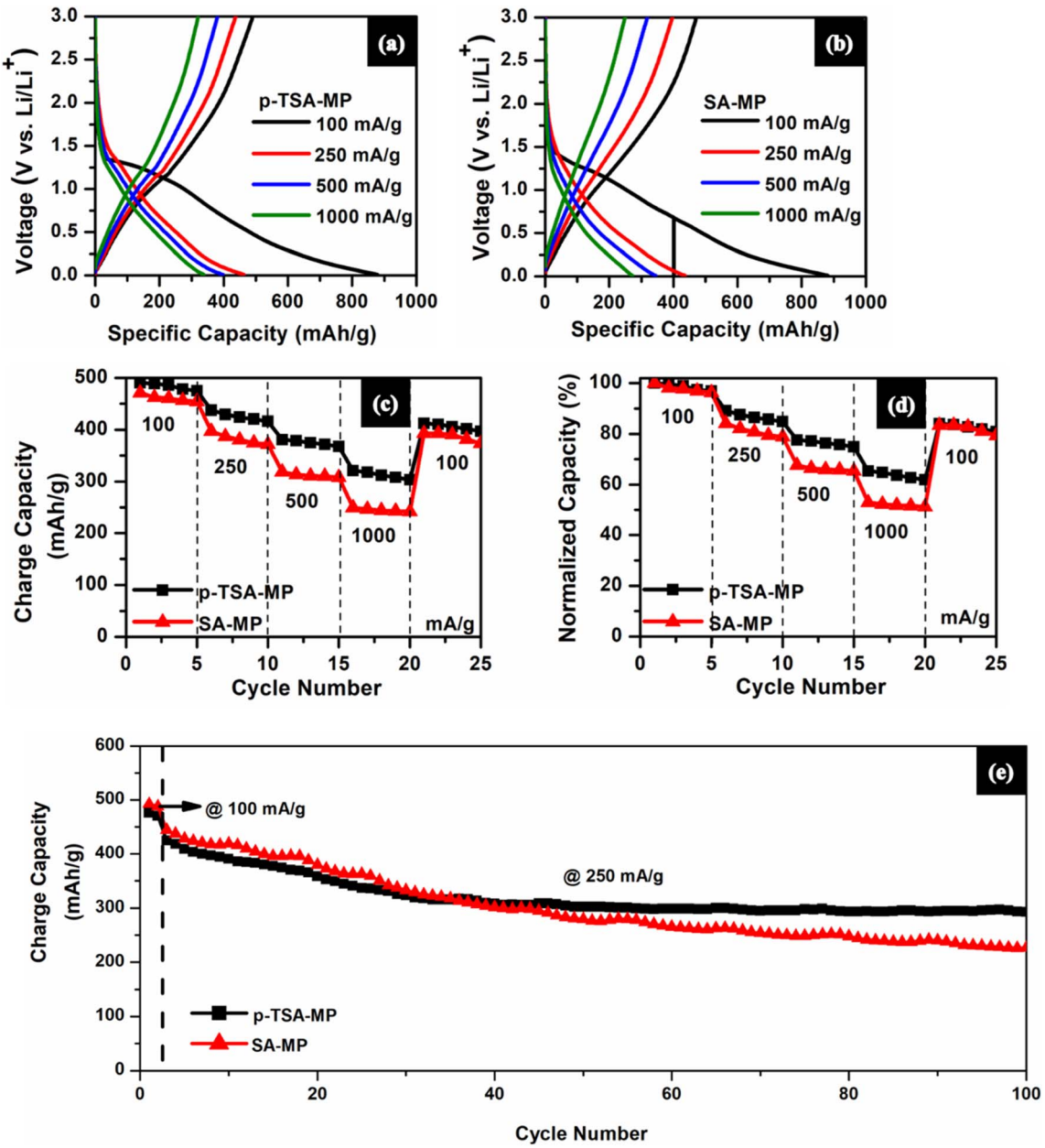

Fig. 5 (a) and (b) The first charge–discharge profile, (c) and (d) the rate performance and normalized capacity (%) and (e) cycling at 100 and 250 mA g^{-1} of mixed metal phosphides for *p*-TSA-MP and SA-MP.

as NiO). While the XRD patterns of mixed metal oxides prepared from two different oxalates (*p*-TSA and SA) in Fig. 2(b) look similar, having the highest intensity peaks at 36° (Co_3O_4/MnO_2 # COD 9016546), 43° and 63° ($NiO/NiMn_2O_4$ # COD 1531194). The XRD data indicates that the materials exhibit a phase-separated form as Ni_xO_y, Mn_xO_y and Co_xO_y. To further characterize and determine the stability of S-NMC, mixed metal oxalates synthesized using two different leachants, *p*-TSA and SA, thermo-gravimetric analysis (TGA) was conducted in a temperature range of 25 °C to 700 °C. It is clear from Fig. S2† that S-NMC has a very much lower weight loss percentage of 7.8%. But the mixed metal oxalates leached from different acids are almost similar in weight loss at around 61% which confirms the oxalate form of the samples in which PTSA and SA show a similar weight loss percentage. The curve can be divided into two stages, where 25 °C to 200 °C represents about 20% weight loss due to dehydration. The second loss, in the 200 °C to 300 °C range, is about 40%, due to carbon burnout and metal oxide formation. Above 300 °C and up to 700 °C, the weight loss was noted to be negligible, confirming the formation of metal oxides.[56,57] Fig. S3a and b† shows the FESEM images of mixed metal oxalate prepared using *p*-TSA and SA, respectively. The oxalate particles exhibit uniformity in size distribution with a minor faceted morphology. Fig. S3c and d† exhibits the oxalates converted to metal phosphides using *p*-TSA and SA, respectively. The *p*-TSA-derived phosphides show an agglomerated primary particle morphology with needle-like features on the surface and the SA-derived ones show agglomerated primary particles without any surface features. Fig. S4a† displays the energy dispersive X-ray spectrum and elemental quantification of an SA-derived mixed metal oxalate sample. The elemental analysis shows that the Ni/Mn at% ratio is consistent with the NMC compound while the Ni/Co at% ratio shows it to be Ni-rich (about 15% higher). When the elemental composition of the phosphides was analyzed, the SA-derived phosphide exhibited a similar at% ratio to that of oxalate (Fig. S4b†); however, the *p*-TSA-derived phosphide exhibited a lower Ni/Mn at% while Ni/Co atomic% was comparable to that of the oxalate (Fig. S4c†). A small amount (0.6–1.2 at%) of aluminum impurity was observed in the metal phosphide samples, but it was not observed in the metal oxalate sample.

Fig. 3(a–c) display the low-magnification TEM images of mixed metal phosphides of *p*-TSA-MP, and mixed metal oxides of *p*-TSA-MO and SA-MO, respectively. Fig. 3(a) shows mostly rod-like structures in which clusters of particles are seen along with tube-like structures. Fig. S3e† exhibits the TEM image of a *p*-TSA-derived metal phosphide sample, which shows mixed small particles with rod-like features. The morphology of mixed metal oxides was spherical in shape with a reasonable degree of agglomeration. The HRTEM of Fig. 3(d) *p*-TSA-MP has an inter-planar spacing of 0.228 nm representing the (111) of hexagonal Ni_2P.[58,59] In Fig. 3(e), *p*-TSA-MO clearly shows lattice fringes with an inter-planar spacing of 0.46 nm corresponding to the (111) of spinel $NiMn_2O_4$. Similarly, for SA-MO in Fig. 3(f), the inter-planar spacing is about 0.47 nm that corresponds to the (111) of spinel $NiMn_2O_4$.[60]

Fig. 4 depicts the surface chemical XPS analysis of S-NMC, *p*-TSA-MP, SA-MP, *p*-TSA-MO and SA-MO samples. Fig. 4(a) shows the C 1s spectra in which the highest peak at 284.6 eV for all the samples represents C–C formation and is also used for spectral calibration. The presence of a small peak at 285.9 eV corresponds to C–O and a broad peak at about 283.2 eV in the SA-MP sample is possibly due to M–C bonds. The C–O bonds originated from the organic compounds used for recycling process. The O 1s spectra confirmed the lattice oxygen peaks at 529.5 eV and peaks in the range of 531.6 eV are attributed to P–O bonds in MP samples. While the surface hydroxyl or C–O bond peak at 531.2 eV of oxide samples and adsorbed O_2 at 533.2 eV are also present in most of the samples.[61] Additionally, in Ni 2p signals, S-NMC has peaks at 854.5 eV and 856.2 eV which can be attributed to Ni^{3+} and Ni^{2+}, respectively, but the majority is in Ni^{2+}, NiO-like phase.[62] For MP samples the Ni 2p peaks have a poor signal/noise ratio but slightly higher binding energy than in metal oxides for Ni^{3+} a more Ni_2P-like phase. Finally for Mn 2p in Fig. 4(d), the binding energy associated with the major peaks is 641.6 eV with a small high-energy shoulder at 643.9 eV both corresponding to Mn^{3+} and Mn^{4+}, respectively, of Mn $2p_{3/2}$ and the peak at 653.4 eV represents Mn $2p_{1/2}$.[63] Additionally, Co 2p, P 2s, P 2p and survey spectra are provided in the ESI (Fig. S5†). In the Co 2p XPS spectra, most samples (except the metal oxide) displayed weak peaks at 780 ($2p_{3/2}$) and 795 eV ($2p_{1/2}$) assigned to cobalt Co^{3+}. In the survey spectrum, all the elemental peaks are visible and confirm its presence in the surface itself. Furthermore, for mixed metal phosphides, the P 2s and P 2p spectra are also added to confirm the formation of phosphides and phosphates on the surface. For P 2s the major peak formed between 190 and 192 eV is consistent with the literature for phosphates[64] and for P 2p, the peak at 135 eV represents surface P–O bonding. Yet the peak position around 133 eV of the *p*-TSA-MP sample is an indication of M–P bonding on the surface.

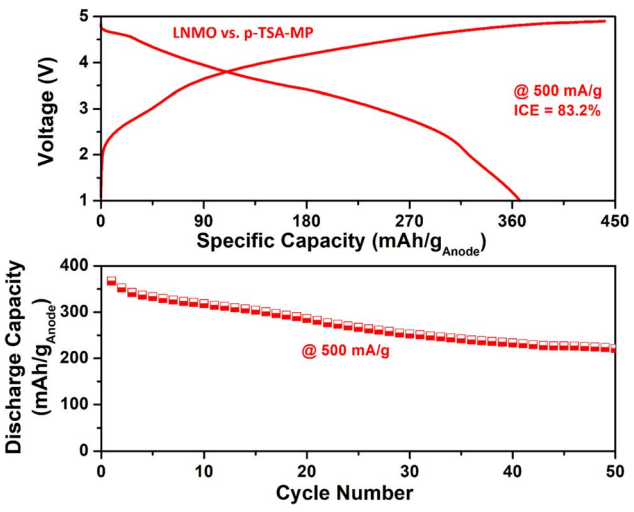

Fig. 6 Electrochemical analysis of LNMO *vs.* *p*-TSA-MP: (a) voltage *vs.* specific capacity (mA h g_{anode}^{-1}) and (b) discharge capacity (mA h g_{anode}^{-1}) *vs.* cycle number of LNMO *vs.* *p*-TSA-MP at a current of 500 mA g^{-1} for 50 cycles.

3.3. Electrochemical studies

3.3.1. Mixed metal phosphides. Fig. 5(a) shows the *p*-TSA-derived mixed metal phosphide in which 878.6 mA h g^{-1} was the first discharge capacity at 100 mA g^{-1} followed by charge capacities of 490.5, 437.5, 380.8 and 320.7 mA h g^{-1} at 100, 250, 500 and 1000 mA g^{-1}, respectively. The first discharge capacity of SA-derived mixed metal phoshide was 881.4 mA h g^{-1} at 100 mA g^{-1} (Fig. 5(b)). The charge capacities at 100, 250, 500 and 1000 mA g^{-1} were 471.1 396.9, 318.5 and 249.2 mA h g^{-1}, respectively. Charge capacity *vs.* cycle number of mixed metal phosphides using two different organic acids, namely *p*-TSA and SA, are displayed in Fig. 5(c). The data was recorded for different specific currents starting from 100, 250, 500 and 1000 mA g^{-1} also after a high rate, it was reverted back to 100 mA g^{-1} and the cells was tested for 5 cycles at each specific current. From this data it is clear that the *p*-TSA-MP sample has more charge capacity than SA-MP at low and high rates. In the case of normalized capacity, the SA-MP sample shows a decay in capacity at higher rates, but *p*-TSA-MP did not show huge variations at either low or high currents. The rate retention (ratio of

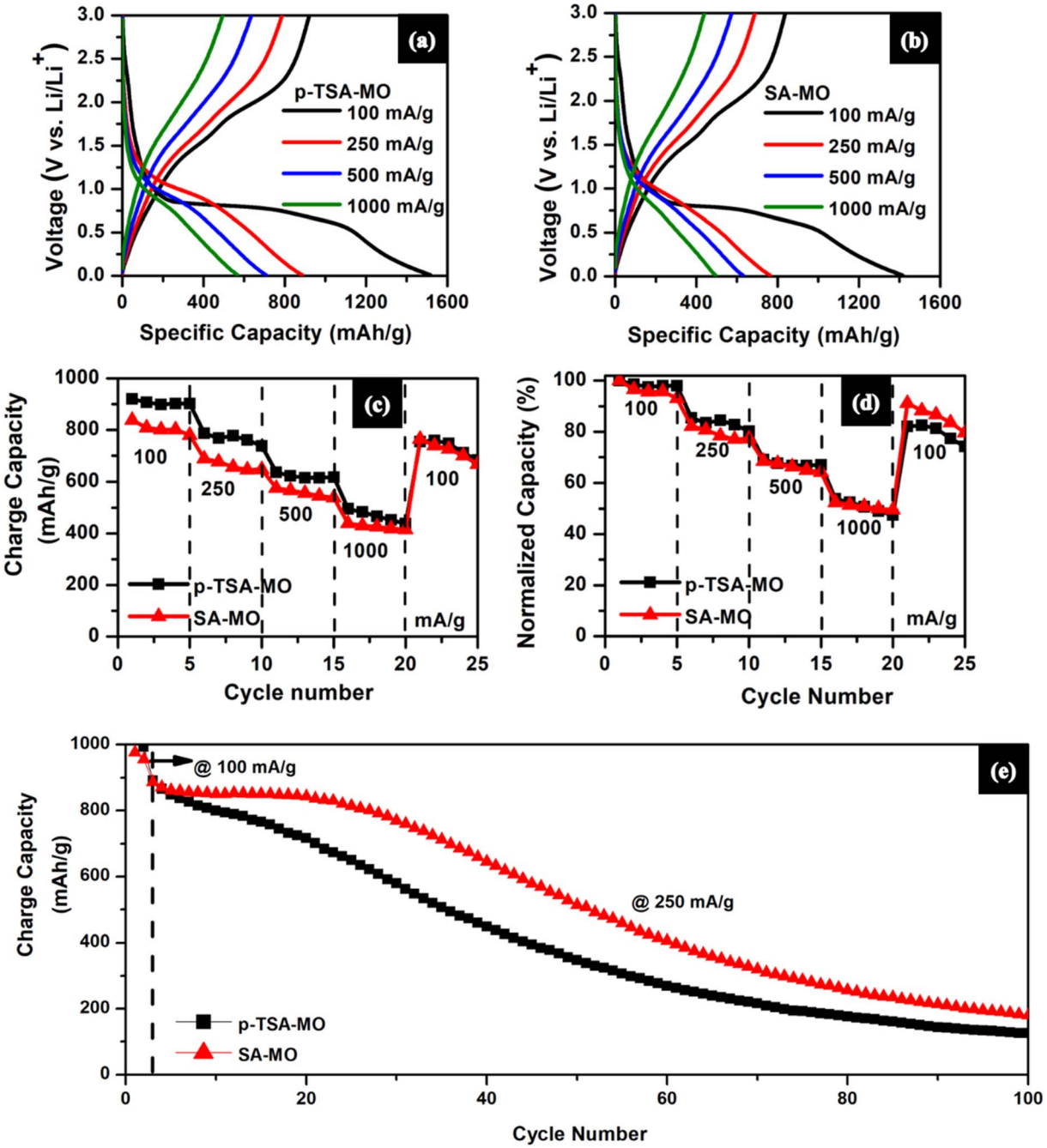

Fig. 7 (a) and (b) The first charge–discharge profile in a voltage window 0.01–3.0 V, (c) and (d) rate performance and normalized capacity (%), and (e) cycling performance cycled at 100 and 250 mA g^{-1} for mixed metal oxides *p*-TSA-MO and SA-MO.

high-rate to low-rate capacity) for *p*-TSA-MP was 69% and that for SA-MP was only 55%, as noted from Fig. 5(d). The cycling performance of two mixed metal phosphides derived from *p*-TSA and SA was tested, in which the first two cycles were cycled at 100 mA g^{-1} and the third cycle onwards at 250 mA g^{-1}. From this cyclic performance in Fig. 5(e), the retention capacity for *p*-TSA is 69% and that for SA is 51% after 100 cycles at 250 mA g^{-1}. It is obvious that *p*-TSA-MP has a relatively better capacity retention than SA-MP. Hence, *p*-TSA-MP was utilized to fabricate a full-cell with a high-voltage LNMO as cathode that was prepared in the lab. Fig. 6 exhibit the results of a full-cell cycled between voltage windows of 1.0 V and 4.9 V at 500 mA g^{-1}. It delivered an initial charge/discharge capacity of 440.8/366.7 mA h g_{anode}^{-1} with initial coulombic efficiency (ICE) of 83.2% with an average voltage of 3.4 V. The initial cycle energy density obtained for LNMO *vs.* *p*-TSA-MP is calculated to be 188.9 W h kg^{-1} (based on the total active weight of the cathode and anode). The full-cell delivered a capacity retention of about 60% at the end of 50 cycles.

3.3.2. Mixed metal oxides. Fig. 7(a) shows the *p*-TSA-MO electrode charge–discharge profiles where the first discharge capacity of 1516.31 mA h g^{-1} at 100 mA g^{-1} was recorded followed by the charge capacities at 100, 250, 500 and 1000 mA g^{-1} of 920.51, 786.75, 635.92 and 494.36 mA h g^{-1}, respectively. The first discharge capacity of SA-MO was 1416.27 mA h g^{-1} at 100 mA g^{-1}, as depicted in Fig. 7(b). The charge capacities at 100, 250, 500 and 1000 mA g^{-1} were 837.80, 688.30, 574.10 and 439.19 mA h g^{-1}, respectively. The *p*-TSA-MO has higher discharge capacity than the SA-MO sample. Fig. 7(c) shows the capacity as a function of cycle number at different rates. From this data it is very clear that at low current density, *p*-TSA-MO has higher capacity than SA-MO; but at 1000 mA g^{-1}, both electrodes exhibit similar capacities.

From the normalized capacity profile (Fig. 7(d)), both *p*-TSA-MO and SA-MO exhibit 60% rate retention. But when it was cycled at 100 mA g^{-1} again, SA-MO exhibited slightly higher capacity than *p*-TSA-MO. From the cyclic performance profile in Fig. 7(e), the initial two cycles were cycled at 100 mA g^{-1} followed by 250 mA g^{-1} for 100 cycles in which at 250 mA g^{-1} *p*-TSA-MO has an initial charge capacity of about 903.97 mA h g^{-1} with 40% capacity retention at the end of 50 cycles and only 14% capacity retention at the end of 100 cycles, while SA-MO exhibits 58% capacity retention at the end of 50 cycles and only 20% capacity retention at the end of 100 cycles with 895.07 mA h g^{-1} initial charge capacity. Such poor cycling stability of bare metal oxides (without any surface engineering or coating) is expected.

Fig. 8 displays the full-cell results of the SA-MO sample against a high-voltage LNMO cathode cycled between 1.5 and 5 V at 500 mA g^{-1}. The cell delivered an initial charge/discharge capacity of 1268.5/957.6 mA h g_{anode}^{-1}, giving an ICE of 75.5% with an average voltage of 3.2 V. From this data, the energy density calculated for LNMO *vs.* SA-MO is 278.6 W h kg^{-1} (based on the total active weight of the cathode and anode). The full-cell delivered a capacity retention of 60% at the end of 50 cycles, which is due to capacity fading of the anode, as noted in the half-cells. These values demonstrate that the recycled anodes when used against suitable cathodes, can produce practically viable Li-ion batteries for potential applications. Furthermore, though the number of cycles reported is limited, the main aim of the present work is only a proof of concept. Tuning the full-cell is necessary to increase cycle life and demonstrate it for fast-charging applications. More process optimization is necessary for practical application of these anode materials (especially the metal phosphides). A strong reducing environment can decrease the P–O and M–O bonds, leading to a high number of M–P bonds that can significantly increase the capacity based on the enhanced alloying reaction of P with Li. Metal oxides have a conductivity problem, high voltage polarization and cycle life issues, as observed here. Yet the anode preparation process is scalable and unlike the pyrometallurgy process, this one exhibits lower energy consumption, enabling practical applications.

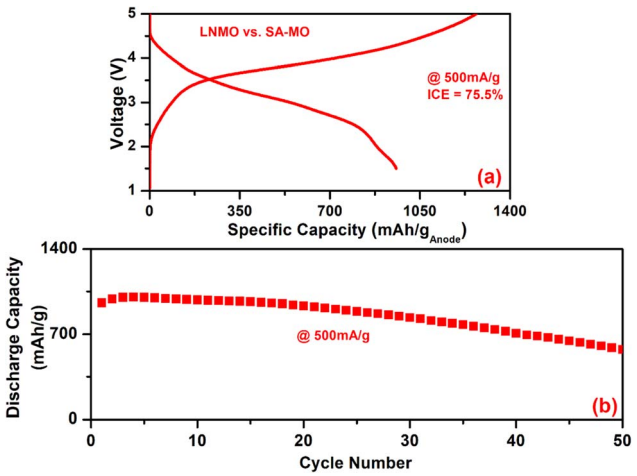

Fig. 8 Electrochemical analysis of LNMO *vs.* SA-MO: (a) voltage *vs.* specific capacity (mA h g_{anode}^{-1}) and (b) discharge capacity (mA h g_{anode}^{-1}) *vs.* cycle number at a current of 500 mA g^{-1} for 50 cycles.

4. Conclusions

The present work focused on the recycling of a spent NMC532 cathode to mixed metal phosphides and oxides as fresh anodes, enabling a circular and sustainable economy. The strategy developed here is to recycle the NMC532 cathode material which is in high demand in the current electronic market. Here, we have for the first time utilized two different environmentally safer acids (compared to sulfuric or hydrochloric acids) to successfully leach out and convert the spent NMC to mixed metal oxalates. A feasible process was demonstrated to convert the mixed metal oxalates to mixed metal phosphides and oxides independently. The recycled compounds have been investigated as LIB anodes and a comparison of the two acids utilized has been studied. The metal phosphides delivered better rate capability, cycle life and reasonable capacity. This work gives insights into the efficient and sustainable process of the conversion of two new acid-based metal oxalates to mixed metal phosphides and metal oxides that has not yet been studied for mixed metal leaching from spent Li-ion battery cathodes. The work demonstrates fresh anodes and full-cells with energy

densities of 188.9 and 278.6 W h kg^{-1} (based on the total active weight of the cathode and anode). Further performance improvements are necessary, as we have demonstrated only 100 cycles with the half-cells and 50 cycles with full-cells. In spite of the high initial capacity, the poor cycle life of metal oxides necessitates surface engineering to address the capacity fading issue. Overall, this work has explored a potential solution for waste management through a sustainable process.

Data availability

The datasets supporting this article have been uploaded as part of the ESI.†

Conflicts of interest

There are no conflicts to declare.

Acknowledgements

Authors are thankful to Amrita Vishwa Vidyapeetham for support.

References

1 S. Windisch-Kern, E. Gerold, T. Nigl, A. Jandric, M. Altendorfer, B. Rutrecht and F. Part, Recycling chains for lithium-ion batteries: A critical examination of current challenges, opportunities and process dependencies, *Waste Manage.*, 2022, **138**, 125–139.
2 B. Gangaja, S. Nair and D. Santhanagopalan, Reuse, recycle, and regeneration of $LiFePO_4$ cathode from spent lithium-ion batteries for rechargeable lithium-and sodium-ion batteries, *ACS Sustain. Chem. Eng.*, 2021, **9**, 4711–4721.
3 F. A. Kayakool, B. Gangaja, S. Nair and D. Santhanagopalan, Li-based all-carbon dual-ion batteries using graphite recycled from spent Li-ion batteries, *Sustainable Mater. Technol.*, 2021, **28**, e00262.
4 F. Degen and M. Schütte, Life cycle assessment of the energy consumption and GHG emissions of state-of-the-art automotive battery cell production, *J. Clean. Prod.*, 2022, **330**, 129798.
5 Q. Wei, Y. Wu, S. Li, R. Chen, J. Ding and C. Zhang, Spent lithium ion battery (LIB) recycle from electric vehicles: A mini-review, *Sci. Total Environ.*, 2023, **866**, 161380.
6 Y. Miao, L. Liu, Y. Zhang, Q. Tan and J. Li, An overview of global power lithium-ion batteries and associated critical metal recycling, *J. Hazard. Mater.*, 2022, **425**, 127900.
7 J. Lin, E. Fan, X. Zhang, R. Chen, F. Wu and L. Li, Sustainable recycling of cathode scrap towards high-performance anode materials for Li-Ion batteries, *Adv. Energy Mater.*, 2022, **12**, 2103288.
8 X. Zhao, B. Peng, C. Zheng and A. Wan, Closed-loop supply chain pricing strategy for electric vehicle batteries recycling in China, *Environ. Dev. Sustain.*, 2022, **24**, 7725–7752.
9 M. Liu, W. Liu, W. Liu, Z. Chen and Z. Cui, To what extent can recycling batteries help alleviate metal supply shortages and environmental pressures in China?, *Sustain. Prod. Consum.*, 2023, **36**, 139–147.
10 M. P. Do, J. J. Roy, B. Cao and M. Srinivasan, Green closed-loop cathode regeneration from spent NMC-based lithium-ion batteries through bioleaching, *ACS Sustain. Chem. Eng.*, 2022, **10**, 2634–2644.
11 J. Neumann, M. Petranikova, M. Meeus, J. D. Gamarra, R. Younesi, M. Winter and S. Nowak, Recycling of lithium-ion batteries—current state of the art, circular economy, and next generation recycling, *Adv. Energy Mater.*, 2022, **12**, 2102917.
12 S. Doose, J. K. Mayer, P. Michalowski and A. Kwade, Challenges in ecofriendly battery recycling and closed material cycles: a perspective on future lithium battery generations, *Metals*, 2021, **11**, 291.
13 A. Manthiram, A reflection on lithium-ion battery cathode chemistry, *Nat. Commun.*, 2020, **11**, 1550.
14 A. Baczyńska, W. Niewiadomski, A. Gonçalves, P. Almeida and R. Luís, LI-NMC batteries model evaluation with experimental data for electric vehicle application, *Batteries*, 2018, **4**, 11.
15 W. Li, E. M. Erickson and A. Manthiram, High-nickel layered oxide cathodes for lithium-based automotive batteries, *Nat. Energy*, 2020, **5**, 26–34.
16 K. H. Chan, J. Anawati, M. Malik and G. Azimi, Closed-loop recycling of lithium, cobalt, nickel, and manganese from waste lithium-ion batteries of electric vehicles, *ACS Sustain. Chem. Eng.*, 2021, **9**, 4398–4410.
17 J. Tan, Q. Wang, S. Chen, Z. Li, J. Sun, W. Liu, W. Yang, X. Xiang, S. Sun and X. Duan, Recycling-oriented cathode materials design for lithium-ion batteries: Elegant structures *versus* complicated compositions, *Energy Storage Mater.*, 2021, **41**, 380–394.
18 Y. Liu, W. Lv, X. Zheng, D. Ruan, Y. Yang, H. Cao and Z. Sun, Near-to-stoichiometric acidic recovery of spent lithium-ion batteries through induced crystallization, *ACS Sustain. Chem. Eng.*, 2021, **9**, 3183–3194.
19 M. Beak, S. Park, S. Kim, J. Park, S. Jeong, B. Thirumalraj, G. Jeong, T. Kim and K. Kwon, Effect of Na from the leachate of spent Li-ion batteries on the properties of resynthesized Li-ion battery cathodes, *J. Alloys Compd.*, 2021, **873**, 159808.
20 Z. J. Baum, R. E. Bird, X. Yu and J. Ma, Lithium-ion battery recycling–overview of techniques and trends, *ACS Energy Lett.*, 2022, **7**, 712–719.
21 X. Zheng, Z. Zhu, X. Lin, Y. Zhang, Y. He, H. Cao and Z. Sun, A mini-review on metal recycling from spent lithium ion batteries, *Engineering*, 2018, **4**, 361–370.
22 S. Kim, J. Bang, J. Yoo, Y. Shin, J. Bae, J. Jeong, K. Kim, P. Dong and K. Kwon, A comprehensive review on the pretreatment process in lithium-ion battery recycling, *J. Clean. Prod.*, 2021, **294**, 126329.
23 A. Beaudet, F. Larouche, K. Amouzegar, P. Bouchard and K. Zaghib, Key challenges and opportunities for recycling electric vehicle battery materials, *Sustainability*, 2020, **12**, 5837.

24 E. Mossali, N. Picone, L. Gentilini, O. Rodrìguez, J. M. Pérez and M. Colledani, Lithium-ion batteries towards circular economy: A literature review of opportunities and issues of recycling treatments, *J. Environ. Manage.*, 2020, **264**, 110500.
25 A. Mohanty, S. Sahu, L. B. Sukla and N. Devi, Application of various processes to recycle lithium-ion batteries (LIBs): A brief review, *Mater. Today: Proc.*, 2021, **47**, 1203–1212.
26 S. Lei, Y. Zhang, S. Song, R. Xu, W. Sun, S. Xu and Y. Yang, Strengthening valuable metal recovery from spent lithium-ion batteries by environmentally friendly reductive thermal treatment and electrochemical leaching, *ACS Sustain. Chem. Eng.*, 2021, **9**, 7053–7062.
27 H. J. Kim, T. N. V. Krishna, K. Zeb, V. Rajangam, C. V. M. Gopi, S. Sambasivam, K. V. G. Raghavendra and I. M. Obaidat, A comprehensive review of Li-ion battery materials and their recycling techniques, *Electronics*, 2020, **9**, 1161.
28 D. Steward, A. Mayyas and M. Mann, Economics and challenges of Li-ion battery recycling from end-of-life vehicles, *Procedia Manuf.*, 2019, **33**, 272–279.
29 S. Sloop, L. Crandon, M. Allen, K. Koetje, L. Reed, L. Gaines, W. Sirisaksoontorn and M. Lerner, A direct recycling case study from a lithium-ion battery recall, *Sustainable Mater. Technol.*, 2020, **25**, e00152.
30 W. Y. Wang, H. C. Yang and R. B. Xu, High-performance recovery of cobalt and nickel from the cathode materials of NMC type li-ion battery by complexation-assisted solvent extraction, *Minerals*, 2020, **10**, 662.
31 J. Lin, L. Li, E. Fan, C. Liu, X. Zhang, H. Cao, Z. Sun and R. Chen, Conversion mechanisms of selective extraction of lithium from spent lithium-ion batteries by sulfation roasting, *ACS Appl. Mater. Interfaces*, 2020, **12**, 18482–18489.
32 E. Gerold, S. Luidold and H. Antrekowitsch, Selective precipitation of metal oxalates from lithium ion battery leach solutions, *Metals*, 2020, **10**, 1435.
33 W. Y. Wang, C. H. Yen and J. K. Hsu, Selective recovery of cobalt from the cathode materials of NMC type Li-ion battery by ultrasound-assisted acid leaching and microemulsion extraction, *Sep. Sci. Technol.*, 2020, **55**, 3028–3035.
34 W. Gao, J. Song, H. Cao, X. Lin, X. Zhang, X. Zheng, Y. Zhang and Z. Sun, Selective recovery of valuable metals from spent lithium-ion batteries–process development and kinetics evaluation, *J. Clean. Prod.*, 2018, **178**, 833–845.
35 W. S. Chen and H. J. Ho, Recovery of valuable metals from lithium-ion batteries NMC cathode waste materials by hydrometallurgical methods, *Metals*, 2018, **8**, 321.
36 W. Gao, X. Zhang, X. Zheng, X. Lin, H. Cao, Y. Zhang and Z. H. I. Sun, Lithium carbonate recovery from cathode scrap of spent lithium-ion battery: a closed-loop process, *Environ. Sci. Technol.*, 2017, **51**, 1662–1669.
37 D. Pant and T. Dolker, Green and facile method for the recovery of spent Lithium Nickel Manganese Cobalt Oxide (NMC) based Lithium ion batteries, *Waste Manage.*, 2017, **60**, 689–695.
38 J. Hu, J. Zhang, H. Li, Y. Chen and C. Wang, A promising approach for the recovery of high value-added metals from spent lithium-ion batteries, *J. Power Sources*, 2017, **351**, 192–199.
39 X. Chen, Y. Chen, T. Zhou, D. Liu, H. Hu and S. Fan, Hydrometallurgical recovery of metal values from sulfuric acid leaching liquor of spent lithium-ion batteries, *Waste Manage.*, 2015, **38**, 349–356.
40 P. Meshram, B. D. Pandey and T. R. Mankhand, Hydrometallurgical processing of spent lithium ion batteries (LIBs) in the presence of a reducing agent with emphasis on kinetics of leaching, *Chem. Eng. J.*, 2015, **281**, 418–427.
41 X. Chen and T. Zhou, Hydrometallurgical process for the recovery of metal values from spent lithium-ion batteries in citric acid media, *Waste Manag. Res.*, 2014, **32**, 1083–1093.
42 J. Li, X. Li, Q. Hu, Z. Wang, J. Zheng, L. Wu and L. Zhang, Study of extraction and purification of Ni, Co and Mn from spent battery material, *Hydrometallurgy*, 2009, **99**, 7–12.
43 J. Liu, T. Y. Mak, Z. Meng, X. Wang, Y. Cao, Z. Lu and Y. Tang, Efficient recovery of lithium as Li_2CO_3 and cobalt as Co_3O_4 from spent lithium-ion batteries after leaching with *p*-toluene sulfonic acid, *Hydrometallurgy*, 2023, **216**, 106012.
44 S. Guo, J. He, L. Zhu, H. Chen, K. Zhou, J. Xu and Z. Chen, Recovery of metallic copper from waste printed circuit boards *via* H_3NO_3S-NaCl-H_2O_2 leaching system, *J. Clean. Prod.*, 2022, **357**, 131732.
45 A. K. Prajapati and A. Bhatnagar, A review on anode materials for lithium/sodium-ion batteries, *J. Energy Chem.*, 2023, **83**, 509–540.
46 J. Deng, S. Wen, J. Deng and D. Wu, Extracting copper from copper oxide ore by a zwitterionic reagent and dissolution kinetics, *Int. J. Miner. Metall. Mater.*, 2015, **22**, 241.
47 M. J. Roldán-Ruiz, M. L. Ferrer, M. C. Gutiérrez and F. d. Monte, Highly Efficient *p*-toluenesulfonic Acid-Based Deep-Eutectic Solvents for Cathode Recycling of Li-Ion Batteries, *ACS Sustainable Chem. Eng.*, 2020, **8**, 5437–5445.
48 B. Lu, R. Du, G. Wang, Y. Wang, S. Dong, D. Zhou, S. Wang and C. Li, High-efficiency leaching of valuable metals from waste Li-ion batteries using deep eutectic solvents, *Environ. Res.*, 2022, **212**, 113286.
49 B. Wang, X. Y. Lin, Y. Tang, Q. Wang, M. K. Leung and X. Y. Lu, Recycling $LiCoO_2$ with methanesulfonic acid for regeneration of lithium-ion battery electrode materials, *J. Power Sources*, 2019, **436**, 226828.
50 S. G. Zhu, W. Z. He, G. M. Li, Z. Xu, X. J. Zhang and J. W. Huang, Recovery of Co and Li from spent lithium-ion batteries by combination method of acid leaching and chemical precipitation, *Trans. Nonferrous Met. Soc. China*, 2012, **22**, 2274–2281.
51 Y. Bai, N. Muralidharan, J. Li, R. Essehli and I. Belharouak, Sustainable direct recycling of lithium-ion batteries *via* solvent recovery of electrode materials, *ChemSusChem*, 2020, **13**, 5664–5670.
52 H. Dong and G. M. Koenig Jr, Compositional control of precipitate precursors for lithium-ion battery active materials: role of solution equilibrium and precipitation rate, *J. Mater. Chem. A*, 2017, **5**, 13785–13798.

53 A. S. Murali, D. S. B. S. Nair and D. Santhanagopalan, Vapour phase conversion of metal oxalates to metal phosphide nanostructures and their use as anode in rechargeable Li, Na and K-ion batteries, *Electrochim. Acta*, 2021, **388**, 138643.

54 M. Walter, M. I. Bodnarchuk, K. V. Kravchyk and M. V. Kovalenko, Evaluation of Metal Phosphide Nanocrystals as Anode Materials for Na-ion Batteries, *Chimia*, 2015, **69**, 724–728.

55 B. Wang, Q. Ru Q. Guo, X. Chen, Z. Wang, X. Hou and S. Hu, Fabrication of one- dimensional mesoporous CoP nanorods as anode materials for lithium-ion batteries, *Eur. J. Inorg. Chem.*, 2017, **2017**, 3729.

56 S. S. Nisa, M. Rahmawati, C. S. Yudha, H. Nilasary, H. Nursukatmo, H. S. Oktaviano, S. U. Muzayanha and A. Purwanto, A fast approach to obtain layered transition-metal cathode material for rechargeable batteries, *Batteries*, 2022, **8**, 4.

57 Y. Zhang, W. Zhang, S. Shen, X. Yan, R. Wu, A. Wu, C. Lastoskie and J. Zhang, Sacrificial template strategy toward a hollow $LiNi_{1/3}Co_{1/3}Mn_{1/3}O_2$ nanosphere cathode for advanced lithium-ion batteries, *ACS Omega*, 2017, **2**, 7593–7599.

58 N. Mushtaq, C. Qiao, H. Tabassum, M. Naveed, M. Tahir, Y. Zhu, M. Naeem, W. Younas and C. Cao, Preparation of a bifunctional ultrathin nickel phosphide nanosheet electrocatalyst for full water splitting, *Sustain. Energy Fuels*, 2020, **4**, 5294–5300.

59 C. Kim, H. Kim, Y. Choi, H. A. Lee, Y. S. Jung and J. Park, Facile method to prepare for the Ni_2P nanostructures with controlled crystallinity and morphology as anode materials of lithium-ion batteries, *ACS Omega*, 2018, **3**, 7655–7662.

60 M. I. A. A. Maksoud, M. A. M. Elsaid and M. A. Elkodous, Gamma radiation induced synthesis of Ag decorated $NiMn_2O_4$ nanoplates with enhanced electrochemical performance for asymmetric supercapacitor, *J. Energy Storage*, 2022, **56**, 105938.

61 T. Yang, L. Pei, S. Yan, Z. Yu, T. Yu and Z. Zouac, In situ formed oxy/hydroxide antennas accelerating the water dissociation kinetics on a Co@N-doped carbon core–shell assembly for hydrogen production in alkaline solution, *Dalton Trans.*, 2019, **48**, 11927–11933.

62 M. Shang, C. Feng, O. G. Shovon and J. Niu, One-pot regeneration and remanufacturing of spent $LiNi_{1-x-y}Mn_xCo_yO_2$ materials with organic acid, *Energy Fuels*, 2022, **36**, 10364–10371.

63 S. Bhowmick, M. K. Mohanta and M. Qureshi, Transcription methodology for rationally designed morphological complex metal oxides: A versatile strategy for improved electrocatalysis, *Sustain. Energy Fuels*, 2021, **5**, 6392–6405.

64 C. D. Wagner, A. V. Naumkin, A. Kraut-Vass, J. W. Allison, C. J. Powell and J. R. Rumble Jr, *NIST Standard Reference Database 20*, 2003.